TÜBİTAK

Turkish Journal of Chemistry

http://journals.tubitak.gov.tr/chem/

Research Article

Turk J Chem
(2017) 41: 440 – 454

doi:10.3906/kim-1610-18

Synthesis of Na-, Fe-, and Co-promoted TiO_2/multiwalled carbon nanotube composites and their use as a photocatalyst

Alp YÜRÜM[1,*], Gürkan KARAKAŞ[2]
[1]Sabancı University Nanotechnology Research and Application Center, İstanbul, Turkey
[2]Department of Chemical Engineering, Middle East Technical University, Ankara, Turkey

Received: 07.10.2016 • **Accepted/Published Online:** 07.01.2017 • **Final Version:** 16.06.2017

Abstract: The use of multiwalled carbon nanotubes (CNTs) in sol-gel synthesized titanium dioxide (TiO_2) photocatalysts as templates was systematically studied. CNTs have high oxidative thermal stability and the controlled removal of CNTs can be achieved at lower temperatures under air flow by the use of Na, Fe, and Co as a catalyst. These catalysts helped to reduce the oxidation temperature of CNTs; thus anatase phase was achieved without significant sintering. The use of a promoter, heat treatment, and various heat treatment atmospheres was effective in specific surface area, crystallinity, and photocatalytic activity against methylene blue (MB) degradation. While the specific surface area of bare TiO_2 was 22 m^2/g, after templating surface areas as high as 191 m^2/g were obtained. For the photocatalytic characterization, with bare TiO_2, the rate constant for MB decomposition was 0.81 h^{-1}, and for CNT–TiO_2 it was 1.31 h^{-1}. Moreover, after Na promotion, the rate constant increased to 1.85 h^{-1}. The results showed that CNTs can be used as a template to tailor and improve the textural properties. Moreover, as a novel material, the Na promotion in CNT–TiO_2 samples showed the best photocatalytic activity by enhancing the interaction between TiO_2 and CNT surfaces.

Key words: Carbon nanotubes, TiO_2, composite, template, sol-gel, anatase, photocatalysis, doping

1. Introduction

Wide band gap semiconductor metal oxides such as TiO_2, ZnO_2, and SnO_2 are widely studied photocatalytic materials for the removal of pollutants in wastewater and air, degradation of organic surface contaminations, disinfection of microorganisms, etc.[1–7] Among these semiconductors, TiO_2 is the prominent photocatalyst due to its stability, nontoxicity, excellent optical and electronic properties, and availability.[8] After examining these advantages, TiO_2 has been considered the most suitable photocatalytic material. Moreover, TiO_2 can be used in various forms such as coatings, thin films, powders, and monoliths that function at room temperature under solar or artificial irradiation.[9–13]

The sol-gel technique is a versatile, low cost, easily controlled wet synthesis method and it is a promising alternative to other techniques based on vacuum deposition processes.[14,15] The colloidal TiO_2 solutions that are obtained by the sol-gel method can be applied as thin films on various substrates such as glass, ceramics, and metals by dip coating, impregnation, or spray coating, leading to the desired composition, thickness homogeneity, adhesion, and appearance.[14,15] The photocatalytic properties of TiO_2 thin films and powders depend on textural and chemical properties such as porosity, surface area, morphology, and crystallinity.[16–19]

*Correspondence: ayurum@sabanciuniv.edu

However, TiO_2 samples obtained by the sol-gel technique are prone to sintering in the vicinity of calcination temperature required for crystallization.[20–25] Sintering is detrimental to the photocatalytic properties of TiO_2 produced by the sol-gel technique, reducing the number of catalytically active defect sites, surface area, and porosity caused by considerable aggregation and grain growth.[24,25] Sintering also favors the phase transition to rutile, which is generally considered less active phase than anatase.[25,26] Sintering can be suppressed by the use of templates and photocatalytically more active TiO_2 samples can be produced using polymers, carbonaceous materials, and surfactants as a template in the sol-gel recipe.[27–32] Therefore, there is a major need for new template materials for TiO_2-based photocatalysts to tailor desired surface area and phases.

Carbon-based materials like carbon nanotubes (CNTs), graphene, and other novel carbonaceous nanomaterials with their unique structures and properties can improve the performance of TiO_2 photocatalysts. CNTs are nanostructured materials having 0.4–2.0 nm diameter with exceptional electronic, mechanical, and thermal properties. The use of multiwalled CNTs as catalyst support is economically advantageous compared to single-walled CNTs and graphene. CNT samples are available in 1–40 nm diameter range. The use of CNT as a support material in CNT–TiO_2 composites has been widely studied in the literature.[33–44] In these studies, the CNT-supported TiO_2 samples exhibit considerably better photocatalytic activity than unsupported TiO_2 although some aggregation and rutile formation were generally reported.[34–42] The photocatalytic activity of TiO_2 is enhanced synergistically by the addition of CNTs due to several mechanisms. CNT–TiO_2 composites have higher surface area than the sol-gel synthesized bare TiO_2 samples. CNTs have higher conductivity and electron storage capacity than TiO_2.[45] Therefore, CNT–TiO_2 composites exhibit lower charge recombination rates because of the favored transfer of excited electrons from TiO_2 to CNTs.[39,42,45] Another possible mechanism is the sensitization of TiO_2 by the transfer of electrons in CNTs into the conduction band of TiO_2.[35] Finally, the formation of C–O–Ti bonds and the resulting favorable energy states is another possible mechanism. The sensitization and the formation of C–O–Ti bonds contribute to the extension of light absorption into the visible region.[36] Therefore, CNT–TiO_2 composites demonstrate higher photocatalytic activity as a result of lower charge recombination rates and the red shift of absorption edge energy toward the visible range.

CNTs have unique thermal resistance even under oxidative conditions. The oxidation temperature of CNT samples varies between 550 and 750 °C, which is limiting the calcination or heat treatment temperature to improve the crystallization during CNT–TiO_2 composite synthesis.[46] In most of the publications, CNT–TiO_2 composite samples were subjected to a heat treatment between 550 and 750 °C, which favors rutile formation and CNT oxidation.[34,38,43,44] Although CNT–TiO_2 composites have been extensively studied in the literature, there are few studies on the use of CNTs as sacrificial or removable templates.[34,43,47] The high thermal stability of CNT materials can be compromised by the presence of impurities including metals to catalyze the degradation of CNTs, especially under oxidative conditions. NaCl is the only known catalyst that lowers the oxidation temperature of CNTs reported in the literature.[48] In addition, Fe and Co catalysts used for CNT growth are reported as impurities that reduce the thermal resistance of CNTs under oxidative atmosphere.[49–51] In addition, Fe and Co are also reported as dopants enhancing the photocatalytic activity of TiO_2.[52,53] Therefore, Na, Fe, and Co can be employed as promoters and catalysts both to achieve the removal of CNT by oxidation at lower temperatures by controlling the phase transformation during the heat treatment and to improve the photocatalytic activity of CNT–TiO_2 composites. In the present study, the use of CNTs as a template was studied for TiO_2 samples synthesized by the sol-gel method. The effects of CNTs on the physical properties and photocatalytic activity were examined. The efficacy of Na, Fe, and Co catalysts for obtaining high surface area TiO_2 photocatalysts by heat treatment under air was tested and the results were compared with

those of CNT–TiO_2 composites that were subjected to heat treatment under an inert atmosphere. Moreover, the effects of CNTs with Na-, Fe-, and Co-promotion on the physical properties and photocatalytic activity of the composites were also studied. It is also important to mention that the CNT–TiO_2–Na composite material is proposed as a novel material and performed significantly better than the other samples.

2. Results and discussion

2.1. Thermal characterization

The thermal properties of the dried TiO_2 and CNT–TiO_2 nanocomposite samples were examined by TGA-DSC analyses. Thermogravimetric analyses of the samples were performed at a heating rate of 10 °C/min under airflow from room temperature to 900 °C. The TGA-DSC curves of bare TiO_2, CNT, and CNT–TiO_2 samples heated in air are presented in Figure 1. The endothermic peaks around 30–380 °C are due to loss of solvents and water by evaporation. The removal of water and organic precursors was completed by 387 °C. The exothermic DTA peak at 417 °C was attributed to the transformation of Ti peroxide species to crystalline anatase, which is in good agreement with the literature.[54] The small exothermic peak observed at 678 °C might be ascribed to anatase–rutile transition. The residual mass was determined as 70% of the initial weight, which was in parallel with the synthesis protocol. The CNT sample was thermally stable until 448 °C under the air flow. The observed sharp weight loss and exothermic DTA peak at 653 °C indicate oxidation of CNTs. The activation energy of CNT oxidation depends on many factors such as the number of walls, defects, and the presence of impurities. In the literature, the oxidation peak for CNT samples is reported to be between 550 and 750 °C.[48,55,56] Total weight loss of 87% was observed and the residual weight was attributed to the impurities in the CNT sample. Figure 1 also shows the thermogravimetric analysis of the CNT–TiO_2 sample. Two-step weight loss was observed for CNT–TiO_2 and its promoted version. These were ascribed to the loss of solvents and water at the low-temperature region and oxidation of CNTs at the higher temperature.

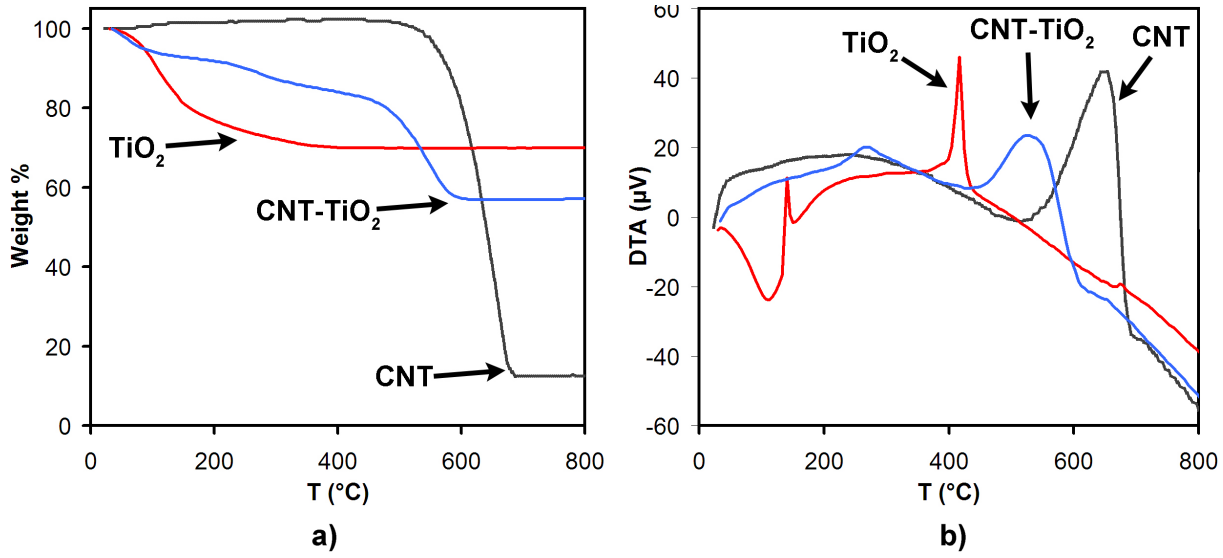

Figure 1. a) TGA and b) DSC data for TiO_2 gel and CNT samples.

The TGA data obtained for samples were normalized with respect to the weight loss obtained for pure TiO_2 by considering the weight of the water–solvent-free sample at 387 °C. Normalized results are then presented in Figure 2a. In addition, the derivative of the TGA data is depicted in Figure 2b. The weight

loss-time data were analyzed by assuming 1st order kinetics and the activation energy of the CNT sample was calculated as 189 kJ/mol using the Coats–Redfern model.[57] The CNT oxidation follows a complex kinetics; in the literature, the activation energy for the oxidation of CNTs is reported to be in the range of 152 to 291 kJ/mol, depending on the purity, tube diameter and length, and thermal–chemical pretreatments.[48,49] On the other hand, a significantly lower activation energy value (130 kJ/mol) was calculated for CNT oxidation in the CNT–TiO_2 sample. This effect may be explained by the catalytic thermal decomposition and oxidation of CNTs in the presence of TiO_2. It is known that defects alone have no effect on oxidation temperature and the number of defects formed under an oxidative environment is not significant. However, the defects associated with the metals and metal oxides accelerate the oxidation of the carbon structure under both oxidizing and reducing conditions.[45,49,58] The hydroxyl groups on the surface of TiO_2 may facilitate the decomposition reaction by reacting with carboxyl groups in CNT surface defects.[58] Similarly, TGA data obtained for Na-, Co-, and Fe-promoted CNT–TiO_2 samples were analyzed and the temperatures determined for 5%, 50%, and 90% weight loss (T_5, T_{50}, and T_{90}), and the activation energies are presented in Table 1. As shown in Figure 2 and Table 1, all TiO_2-containing samples exhibit lower activation energies than bare CNTs. NaCl is reported as an effective catalyst for CNT oxidation. In the literature, the activation energy of CNT oxidation with NaCl is reported as 36–44 kJ/mol at lower temperatures and 170–171 kJ/mol at higher temperatures.[48] The calculated activation energy for the Na-containing sample in this study (159 kJ/mol) lies between those values. We did not observe any double peaks in the DTA curve for Na as reported by Endo et al. The reason is probably that the Na percentage in this study is higher with respect to CNTs.

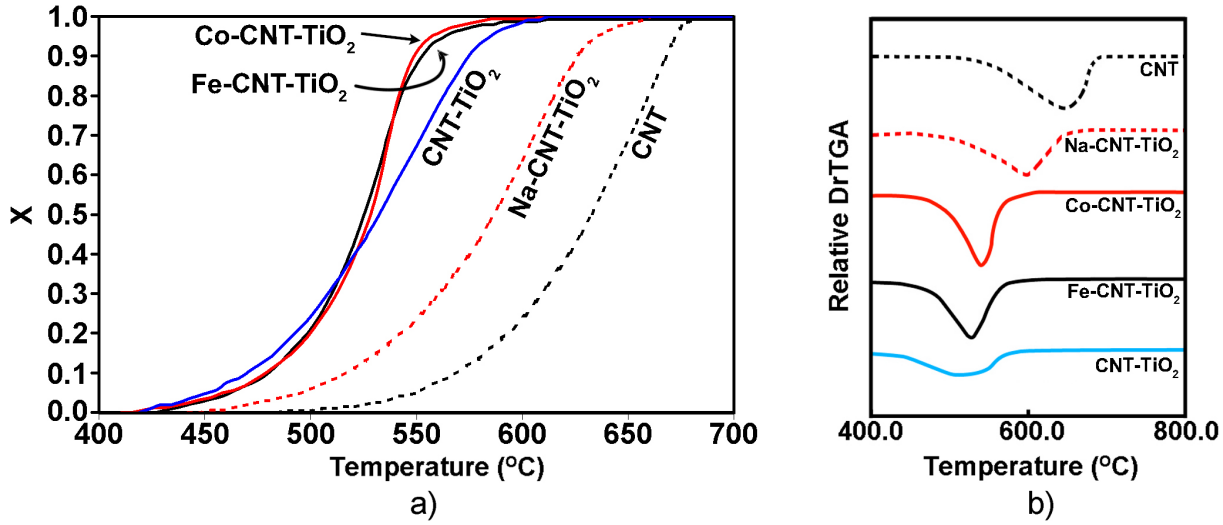

Figure 2. a) TGA data of CNT–TiO_2 samples as fractional weight loss vs. temperature and b) derivative of TGA data of the same samples.

NaCl–CNT–TiO_2 samples require higher temperatures for 5%, 50%, and 90% weight loss compared with the CNT–TiO_2 sample. The detrimental effect of NaCl on TiO_2 can be attributed to the poisoning of TiO_2 by the presence of NaCl or the formation of Na_xTiO_2 species. Fe and Co are reported as good catalysts for CNT growth and known to reduce the thermal stability of CNTs in the presence of oxygen.[50,51] Although lower activation energies were observed for both Fe and Co compared to bare CNTs, the catalytic activity of TiO_2 was reduced by the addition of Fe and Co. This effect is more significant for the latter. On the other hand,

Table 1. Temperatures corresponding 10%, 50%, and 90% weight loss of CNT and activation energies obtained from TGA data of samples.

Sample	T_{10} (°C)	T_{50} (°C)	T_{90} (°C)	Peak oxidation temperature (°C)	Ea (kJ/mol)
CNT	569	632	667	652	189
CNT–TiO_2	471	531	574	524	130
Na–CNT–TiO_2	516	587	626	597	159
Fe–CNT–TiO_2	481	526	553	528	169
Co–CNT–TiO_2	480	528	549	531	185

when TGA curves and peak temperatures are considered, it can be clearly seen that presence of Fe and Co favors the CNT oxidation reaction by pre-exponential factors. The increase can be attributed to the presence of higher number of active sites and surface coverage, which enhance the oxidation rate at lower temperatures than bare CNTs. The formation of hot spots during oxidation is another possible mechanism. Therefore, the interaction of defect sites with Fe and Co atoms enhances the oxidation reaction rate.[55]

2.2. Morphology and crystal structure

The effect of the heat treatment temperature on the morphology of the samples under oxidative and inert atmosphere was investigated by SEM imaging. In Figure 3, the representative SEM images of Na–CNT–TiO_2 samples are depicted. The sample that was treated at 400 °C in nitrogen atmosphere exhibits a fibrous structure composed of intact CNTs and TiO_2 phase (Figure 3a). The fibrous structure was preserved after the calcination in air at 400 °C, indicating the presence of thermally stable CNTs (Figure 3b). At that stage, the fibrous CNT/TiO_2 composite started to form a sponge-like structure with 0.3–1.2-μm wall thickness and 1.1–2.5-μm pores. Actually, the walls of this composite structure consist of smaller pores in the range of 30–220 nm. Higher calcination temperatures in the air lead to disappearance of the fibrous structure to a great extent (500 °C). Complete removal of CNTs was observed at 570 °C, exhibiting a more uniform homogenous structure (Figures 3c and 3d). Even after the removal of the CNTs, the porous structure was preserved. In this case, instead of CNT–TiO_2 composite structure, the walls of the sponge-like structure consist of TiO_2 nanoparticles with a size range of 50–150 nm. Although similar morphologies were also observed for Co and Fe-promoted and bare CNT–TiO_2 samples, the Na-promoted sample had a more homogeneous composite structure. In the other samples (bare, Co-, and Fe-promoted), in some places micron-sized TiO_2 agglomerates without any CNT were observed. This suggests that in Na-promoted samples, TiO_2 had better contact with CNTs.

The specific surface areas of TiO_2, CNT, and CNT–TiO_2 samples are summarized in Table 2. The heat treatment of the pure TiO_2 sample synthesized by the sol-gel method at 400 °C in nitrogen flow resulted in a small surface area due to pore blockage. The calcination in air flow improved the surface area significantly as a result of the better removal of organic precursors and solvents added during the synthesis. Broad pore size distribution of 0.25–0.90 nm was observed for the samples without CNTs and this indicates lack of mesoporosity. The CNT addition significantly improved the specific surface area of all samples. The CNT–TiO_2–Na sample had the highest surface area among the thermally treated samples at 400 °C and this may be attributed to the good contact between TiO_2 and CNTs. According to the TGA and SEM results, a significant portion of CNTs was expected to remain intact after the heat treatment at 400 °C especially in the absence of oxygen. Therefore, the high surface areas of the heat-treated and calcined samples at 400 °C can be attributed to the presence

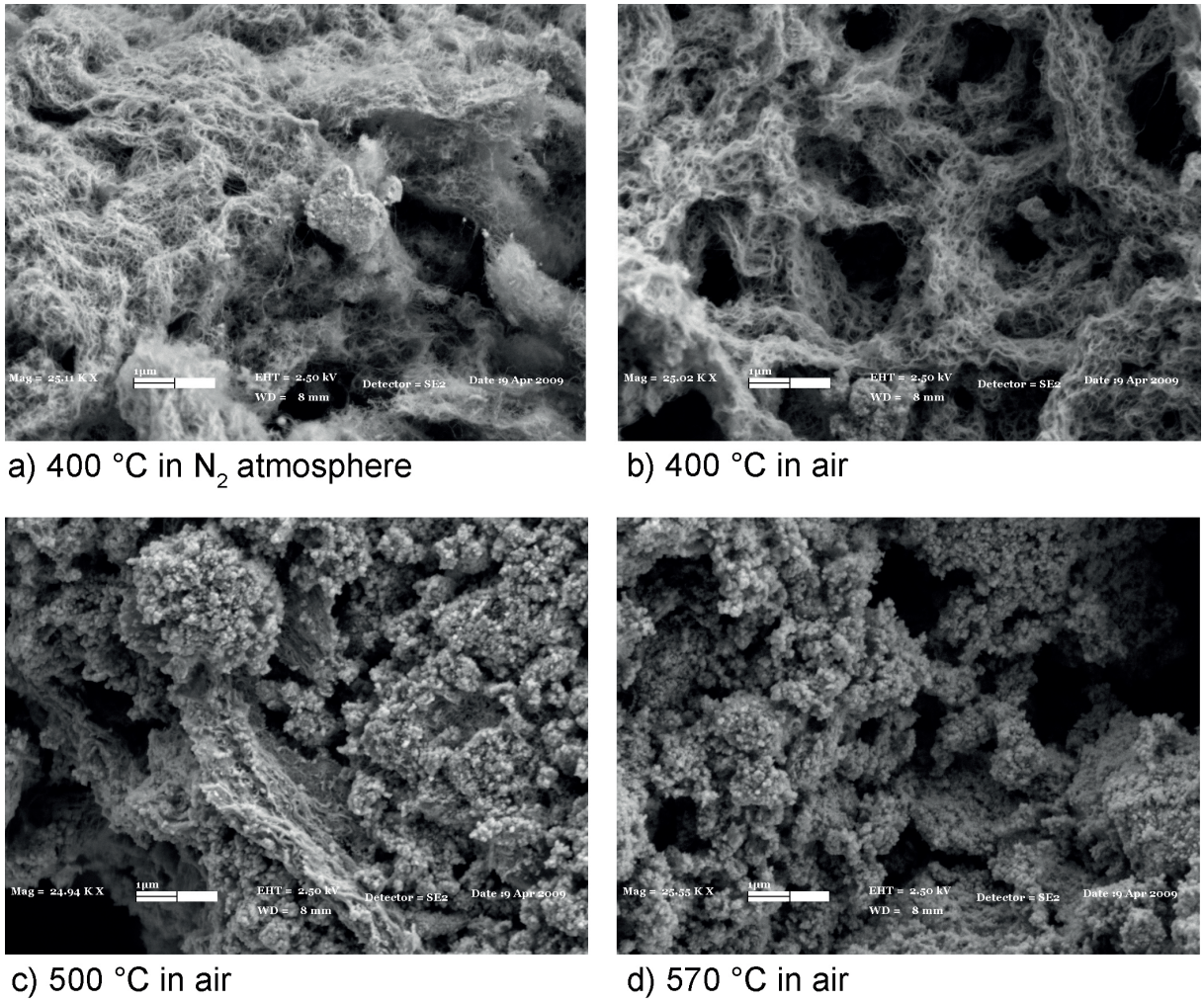

Figure 3. SEM images of CNT–TiO_2–Na heat treated at a) 400 °C with N_2, and calcined at b) 400 °C, c) 500 °C, and d) 570 °C.

of CNTs. However, the larger surface area of the samples calcined at higher temperatures (500 and 570 °C) than pure TiO_2 can be ascribed to the oxidation/fragmentation of CNTs and inhibition of both sintering and particle growth under oxidative conditions. The effect of CNT templating on the morphology is also shown in Figure 4. Under normal conditions, after sol-gel synthesis and calcination, the obtained powder samples had a very dense structure with almost no porosity.[59,60] In our case, thanks to CNTs and metal promotions, highly porous structures were obtained at lower temperatures.

The residual amounts of CNTs in heat-treated and calcined samples were quantified by CHO elemental analysis. The carbon content of CNT–TiO_2–Na samples that were heat-treated and calcined at 400 °C was determined as 33.8% and 22.2%, respectively. The oxidation of CNTs was favored by calcination temperature as expected and 10.0% and 0.1% carbon were measured in CNT–TiO_2–Na samples calcined at 500 °C and 570 °C, respectively. In addition, hot spot formation in the proximity of the catalyst particles should be regarded as an important factor for sintering. Although sintering leads to densification and significant loss of surface area, the resulting surface areas of CNT–TiO_2 composites were still significantly higher than that of the bare

Table 2. The effect of calcination temperature on the BET surface area of CNT templated titania samples.

Sample	Heat treated in N_2 400 °C (m^2/g)	Calcined in air 400 °C (m^2/g)	Calcined in air 500 °C (m^2/g)	Calcined in air 570 °C (m^2/g)
TiO_2	10	22	20	20
CNT–TiO_2	96	105	55	46
Na–CNT–TiO_2	153	162	84	58
Fe–CNT–TiO_2	135	133	73	47
Co–CNT–TiO_2	146	191	68	63
Specific surface area of CNTs (m^2/g)*	250–300			

*Obtained from the manufacturer

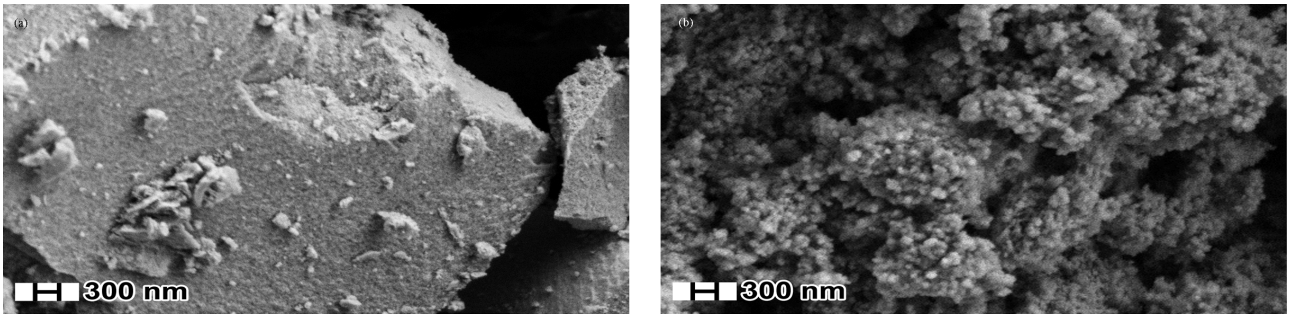

Figure 4. SEM images of a) TiO_2 and b) CNT–TiO_2–Na calcined at 570 °C.

TiO_2 sample. Therefore, the surface area of the CNT–TiO_2 composites can be enhanced by partial removal of CNTs between 400 and 500 °C in air flow.

The XRD analysis of bare and Na-, Co-, and Fe-promoted CNT–TiO_2 samples was carried out to check the possible effect of promoter and heat treatment or calcination conditions on the crystallinity of TiO_2. The XRD spectra of all samples indicate the presence of pure anatase phase with the main (101) peak located at 25.3° for all samples (Figure 5). The crystallinity is enhanced at elevated temperature and by the presence of air.

For CNTs, the main peak is located at 26.1°. This peak corresponds to the (002) plane of graphite and is due to the stacking of graphene sheets in the multiwalled CNT. For all of the CNT–TiO_2 composites, the CNT peak for CNTs could not be clearly observed. The main reason for this is the overlapping of the CNT main peak with the anatase main peak.

On the other hand, for the Fe- and Co-promoted samples, a shift of the (101) peak to lower 2-theta values was observed (Figures 5 and 6). This means that the lattice was expanded due to the introduction of larger Fe and Co atoms.[61,62] Although for the Na-promoted sample no apparent shift was observed, it is acceptable not to see any shift after doping with smaller atoms (Figure 7).[63]

Figure 8 shows the Raman spectra of CNT–TiO_2 composite material. In the left part of the spectrum, the peaks at 144, 196, 395, 513, and 636 cm^{-1} represent the anatase phase of TiO_2. At 1346 and 1595 cm^{-1} a pair of peaks were observed and these peaks correspond to D and G band vibrations, respectively. The D band at 1346 cm^{-1} is related to the defects present in the graphite-based materials like CNTs or graphene. On the other hand, the G band, which is located at 1595 cm^{-1}, is attributed to tangential mode vibrations of C atoms

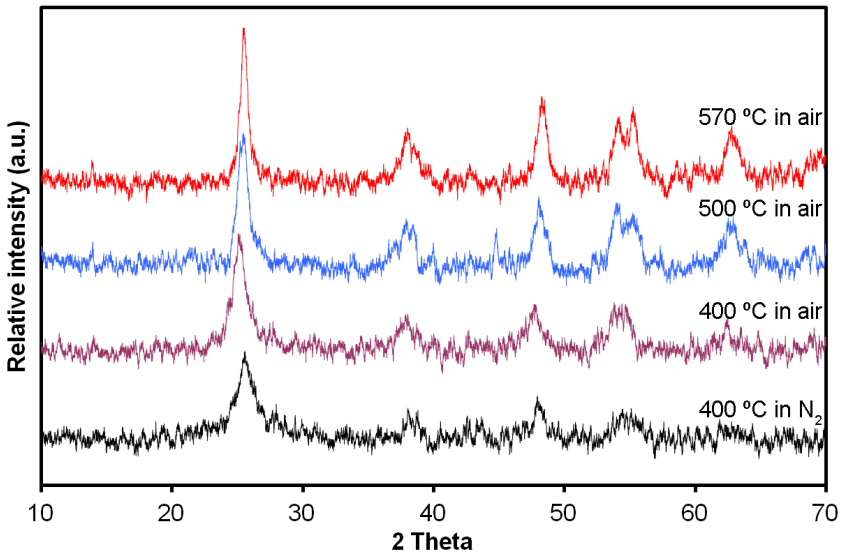

Figure 5. XRD patterns of heat-treated and calcined Fe–CNT–TiO_2 samples.

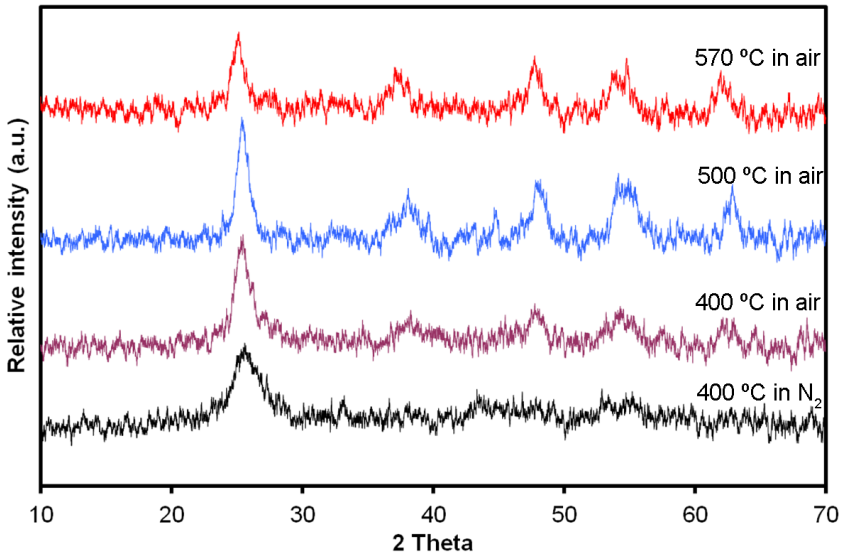

Figure 6. XRD patterns of heat-treated and calcined Co–CNT–TiO_2 samples.

in graphite-based materials. The Raman spectra confirm the presence of anatase phase and its compliance with CNTs in the composite structure.

2.3. Photocatalytic activity

The photocatalytic activities of the samples were evaluated for the degradation of 2 ppm MB solution under 300 W/m^2 artificial solar irradiation at 25 °C by using 1 g TiO_2/L catalyst concentration. The time course of MB concentration was determined by measuring the absorbance of the reaction mixture at 665 nm by UV-Vis spectrometer. The reaction progress for the photocatalytic degradation of MB over the catalyst samples treated under an inert atmosphere at 400 °C is shown in Figure 9. The kinetic data were analyzed and first-order reaction kinetics was observed for all tested catalyst samples. The rate constants calculated for first-order

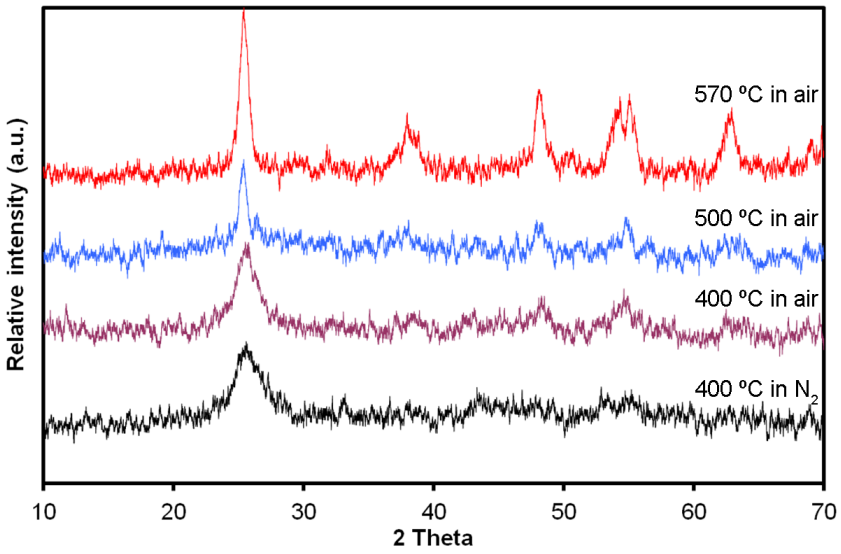

Figure 7. XRD patterns of heat-treated and calcined Na–CNT–TiO_2 samples.

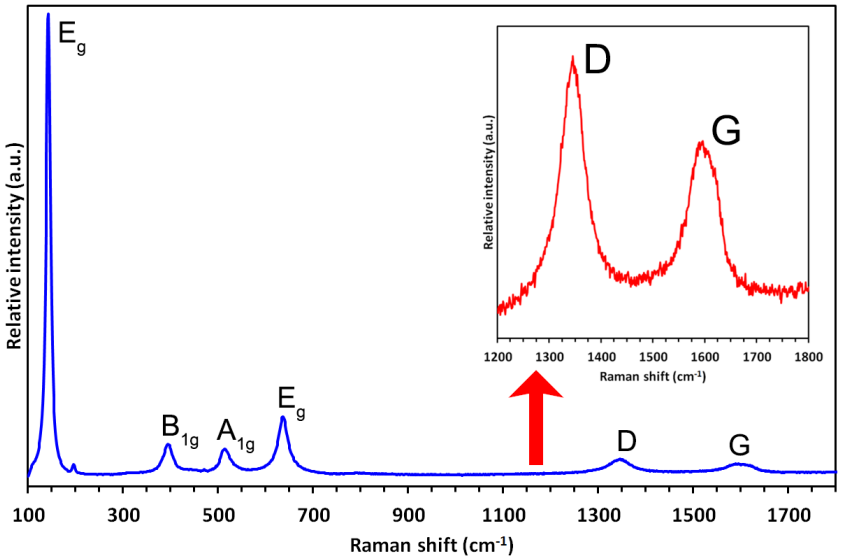

Figure 8. Raman spectra of CNT–TiO_2 composite material (inset: close-up of D and G bands).

reaction kinetics are presented in Table 3. The bare TiO_2 sample exhibited the lowest photocatalytic activity and its activity decreased with increasing calcination temperature. This activity loss can be related to the sintering of the already dense TiO_2 structure. The addition of CNT improved the photocatalytic activity of TiO_2 depending on the heat treatment conditions. The activity of CNT–TiO_2 even without any promotion was increased 1.6 times compared to the bare TiO_2. Actually, this result is close to the literature results. Similarly, in one study, with 20% CNT loading, the activity of CNT–TiO_2 for MB degradation prepared under 24 h of hydrothermal treatment was increased 1.6 times.[64] It is possible to increase the activity even more with higher CNT loadings but it is not feasible to use that much CNTs for a practical application.[65] The highest activity was observed for the Na–CNT–TiO_2 sample treated at 400 °C in N_2 (1.85 h^{-1}) where complete conversion was achieved in 3 h. The effect of CNT addition significantly receded with increasing calcination temperature.

However, even at 570 °C, where no CNTs were present in the sample, the activity was still higher than that of the bare TiO_2. At that condition, with Na-promotion, the activity is 1.2 times higher than with pure TiO_2. Interestingly, Yang et al. also obtained that much enhancement after 1% of Na addition.[63] The enhanced photocatalytic activity can be explained by the increase in surface area and synergy caused by the doping, good contact, and electron transfer with sensitization mechanisms.[35,39,42,45]

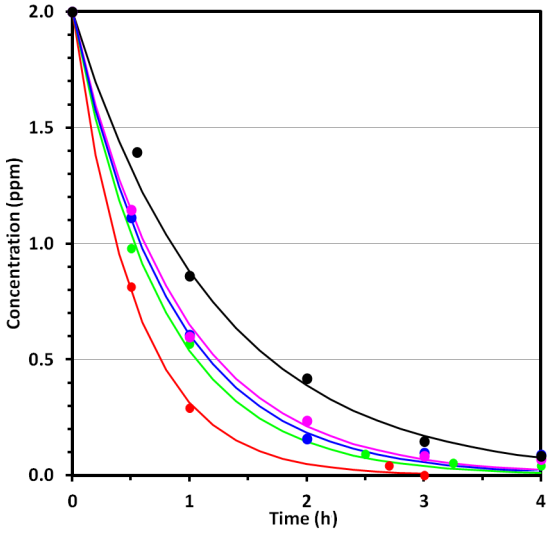

Figure 9. Photocatalytic activity of samples heat treated @ 400 °C (0.1 L solution, 1 g TiO_2/L, 300 W/m^2 irradiation) (red, CNT–TiO_2–Na; green, CNT–TiO_2; blue, CNT–TiO_2–Co; purple, CNT–TiO_2–Fe; black, TiO_2).

Table 3. The effect of calcination conditions on the initial rate constants of photocatalytic decomposition of MB.

Sample	Heat treated in N_2 @ 400 °C (h^{-1})	Calcined in air @ 400 °C (h^{-1})	Calcined in air @ 500 °C (h^{-1})	Calcined in air @ 570 °C (h^{-1})
TiO_2	0.81	0.82	0.71	0.64
CNT–TiO_2	1.31	1.28	0.95	0.62
Na–CNT–TiO_2	1.85	1.44	0.89	0.79
Fe–CNT–TiO_2	1.14	0.82	0.51	0.53
Co–CNT–TiO_2	1.19	1.01	0.57	0.60

Catalyst samples heat treated under nitrogen flow at 400 °C exhibited better photocatalytic activities compared to those calcined in the air and at higher temperatures in spite of their lower specific surface area values. CNT–TiO_2, Na–CNT–TiO_2, and Co–CNT–TiO_2 samples calcined in air at 400 °C exhibited higher surface areas than their counterparts treated in N_2 at 400 °C. The reduction in catalytic activity with the increase in surface area can be explained by the loss of active sites and intimate contact between TiO_2 crystallites and CNT walls. The heat treatment promotes the incorporation of TiO_2 into CNT walls and the presence of oxygen induces the fragmentation of graphitic structure. These results indicate that there is a strong interaction between TiO_2 crystallites and CNT. Moreover, TiO_2 catalyzes the oxidation of CNT during heat treatment.

When Na-, Fe-, and Co-promoted samples are considered, the highest activity was observed for the Na–CNT–TiO_2 sample heat treated in N_2 at 400 °C (Figure 10). These results are in good agreement with the retardation effect of sodium on fragmentation, oxidation observed in TGA results, and the high surface area.

On the other hand, for some cases, sodium is a known poison for TiO_2 photocatalysts. There are various debates on the effect of Na ions on the structure and photocatalytic activity of TiO_2.[66–68] Sodium diffusion from glass substrates causes disorders in TiO_2 crystallites acting as charge recombination centers. In addition, the formation of large crystallites and the retardation of anatase formation are also reported. However, no adverse effect of sodium on the surface area, crystallization, or photocatalytic activity was observed for Na–CNT–TiO_2 samples, which can be explained by the low Na content, low cohesive energy, and favored adsorption of sodium ions into CNT walls.[69] Although Fe- and Co-promoted CNT–TiO_2 samples have higher surface area than bare TiO_2, their photocatalytic activities are significantly lower than the unpromoted CNT–TiO_2 sample. This effect is more pronounced in the presence of oxygen at 400 °C. There are various studies revealing the desired and deleterious effects of Fe- and Co-promoters in TiO_2 photocatalysts and the activity depends on both loading and the dispersion of these metals. After a certain level of doping, metal sites act as charge recombination centers.[53]

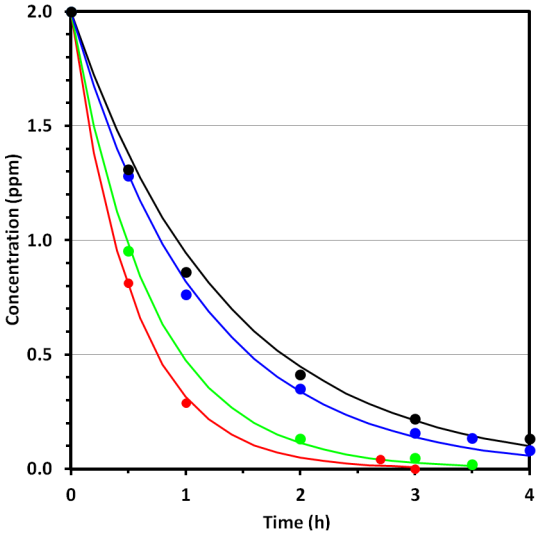

Figure 10. Photocatalytic activity of CNT–TiO_2–Na group samples (0.1 L solution, 1 g TiO_2/L, 300 W/m^2 irradiation) (red, CNT–TiO_2–Na heat treated @ 400 °C; green, CNT–TiO_2–Na calcined @ 400 °C; blue, CNT–TiO_2–Na calcined @ 500 °C; black, CNT–TiO_2–Na calcined @570 °C).

As a result, different heat treatment processes can be applied to tailor the morphology and photocatalytic activity of CNT–TiO_2 composites. The surface area of the composites can be enhanced by the addition and controlled removal of CNTs. TiO_2 phase catalyzes the oxidation of CNTs in the presence of oxygen. The addition of Na, Fe, and Co induces CNT fragmentation and forms active sites for photocatalytic reactions.

From the Na-promotion point of view, the introduction of alkali atoms creates strong basic sites on the catalyst surface.[70,71] These sites can be highly active places for photocatalysis. The material can create the basic sites according to the following reaction Eq. (1):

$$-Ti-O-Na \rightarrow -Ti-O^- + Na^+ \tag{1}$$

The creation of these basic sites may also enhance the adsorption of MB and the injection of its electrons to the conduction band of TiO_2 (and later onto CNTs) under UV irradiation. The injected electron can further react with surface O_2 and yield $O_2^{\cdot-}$ radicals and increase the degradation rate.

Moreover, at lower loadings, Na acts as a shallow electron trap and enhances the electron transfer from the TiO_2's valence band to its conduction band. This eventually results in radical formation for photodegradation.[72]

3. Experimental

3.1. Sample preparation

TiO_2 samples were synthesized by the hydrolysis of 8.4 mL of titanium tetra-isopropoxide (TTIP) (Aldrich, extra pure grade) in 20 mL of ethanol (Aldrich, C_2H_5OH, 99.5%) by the addition of 0.5 mL of 1% HCl solution in a thermostated bath at 0 °C with continuous stirring for 1 h. Bare TiO_2 samples were prepared by drying the solution overnight at 60 °C in an oven. CNT–TiO_2 nanocomposites were synthesized by mixing the appropriate amount of CNTs (Nanocyl NC7000, 9.5 nm average diameter, 1.5 μm average length, and 250–300 m^2/g surface area) with the TiO_2 sol to achieve 40 wt% CNT loading in an ultrasonic bath for 20 min at room temperature. After sonication, the mixture was dried overnight at 60 °C in an oven. The catalytic oxidation of CNTs was tested by Na, Fe, and Co as promoters. For this purpose, appropriate amounts of $FeCl_3$, $CoCl_2$, and NaCl (for all of the salts the brand was Merck) aqueous solutions were added to the mixture during ultrasonication to achieve 1% Na, Fe, and Co loading. Heat treatment of the samples was performed under N_2 flow at 400 °C for 120 min in a tube furnace. Similarly, the calcination of the samples was carried out of at 400, 500, and 570 °C under airflow for 120 min.

3.2. Sample characterization

The crystal structure was analyzed by X-ray diffractometer (Philips, PW 1840) with Cu target and Ni filter (Cu Kα = 1.5418 nm). The surface imaging was performed by scanning electron microscopy (SEM, Gemini Leo, Supra 35VP). The BET specific surface areas of the samples were determined by N_2 sorption (Micromeritics-Gemini V Series). Moreover, to compare the metals added and their catalytic effects, TGA-DTA analyses were performed by Shimadzu DSC-60 with a 10 °C/min heating rate under air flow. Raman results were recorded from the samples by utilizing a Renishaw Raman spectrometer (532 nm laser).

3.3. Photocatalytic activity measurement

Photocatalytic activities of the samples were tested by the photodegradation of methylene blue (MB) solution. For this purpose, 300 mL of 2 ppm MB (Merck) solution was irradiated under 300 W/m^2 artificial solar irradiation (Suntest CPS+, Atlas) for 4 h. The solar simulator was equipped with a xenon lamp and a soda-lime glass filter (320–800 nm) and the irradiation chamber was kept at 25 °C during the reaction tests. The MB degradation was followed by the analysis of samples from the reaction mixture using a UV-Vis spectrophotometer (Shimadzu) calibrated at 665 nm.

4. Conclusion

The use of multiwalled CNTs as a template for the synthesis of high surface area TiO_2 photocatalysts was investigated and the photocatalytic activity of the templated TiO_2 samples was compared with that of bare TiO_2 photocatalysts. The catalytic performances of Na, Fe, and Co on the oxidation temperature of CNTs were examined under oxidative and inert atmospheres. Controlled removal of CNTs was achieved at lower temperatures and nanocomposites composed of anatase TiO_2 and CNT fragments were obtained. The presence of Na, Fe, Co, and TiO_2 has an important role in the thermal oxidative stability of CNTs by reducing the

activation energy and increasing the pre-exponential factor and surface area. As a result, CNTs can be employed as a removable template for tailored CNT–TiO_2 photocatalysts leading to high specific surface area samples with desired photocatalytic activity and morphological properties.

In addition, TiO_2–CNT composites treated under inert atmosphere had better photocatalytic activity than the samples treated in air flow, which is explained by the synergy between CNTs and TiO_2. While Co- and Fe-promoted samples demonstrated lower photocatalytic activity than the bare TiO_2 and CNT–TiO_2 samples due to the formation of charge recombination centers, the highest photocatalytic activity was obtained with the Na-promoted sample. More specifically, Na helped to create better contact between TiO_2 and CNTs. This is crucial for efficient electron transfer. Moreover, the low Na loading enhanced the photocatalytic degradation of MB by creating strong basic sites and helping electron transfer. The rate constants of bare TiO_2, CNT–TiO_2, and CNT–TiO_2–Na were calculated to be 0.81, 1.31, and 1.85 h^{-1} respectively. As far as we know, CNT–TiO_2–Na composite has never been introduced before in the literature and the activity increase obtained with that sample is quite promising.

Acknowledgments

We acknowledge the financial support from the METU Scientific Research Fund and Sabancı University Nanotechnology Research and Application Center for the SEM imaging.

References

1. Erdural, B. K.; Yurum, A.; Bakir, U.; Karakas, G. *J. Nanosci. Nanotechno.* **2008**, *8*, 878-886.
2. Zheng, H.; Maness, P. C.; Blake, D. M.; Wolfrum, E. J.; Smolinski, S. L.; Jacoby, W. A. *J. Photoch. Photobio. A* **2000**, *130*, 163-170.
3. Mills, A.; Davies, R. H.; Worsley, D. *Chem. Soc. Rev.* **1993**, *22*, 417-425.
4. Erkan, A.; Bakir, U.; Karakas, G. *J. Photoch. Photobio. A* **2006**, *184*, 313-321.
5. Tseng, T. K.; Lin, Y. S.; Chen, Y. J.; Chu, H. *Int. J. Mol. Sci.* **2010**, *11*, 2336-2361.
6. Vaiano, V.; Iervolino, G.; Sannino, D.; Murcia, J. J.; Hidalgo, M. C.; Ciambelli, P.; Navio, J. A. *Appl. Catal. B-Environ.* **2016**, *188*, 134-146.
7. Bernardini, C.; Cappelletti, G.; Dozzi, M. V.; Selli, E. *J. Photoch. Photobio. A* **2010**, *211*, 185-192.
8. Diebold, U. *Surf. Sci. Rep.* **2003**, *48*, 53-229.
9. Paz, Y.; Luo, Z.; Rabenberg, L.; Heller, A. *J. Mater. Res.* **1995**, *10*, 2842-2848.
10. Hasegawa, G.; Kanamori, K.; Nakanishi, K.; Hanada, T. *J. Am. Ceram. Soc.* **2010**, *93*, 3110-3115.
11. Hu, L. L.; Yoko, T.; Kozuka, H.; Sakka, S. *Thin Solid Films* **1992**, *219*, 18-23.
12. Guan, K. H. *Surf. Coat. Tech.* **2005**, *191*, 155-160.
13. Orha, C.; Manea, F.; Pop, A.; Bandas, C.; Lazau, C. *Desalin. Water. Treat.* **2016**, *57*, 14178-14187.
14. Ahn, Y. U.; Kim, E. J.; Kim, H. T.; Hahn, S. H. *Mater. Lett.* **2003**, *57*, 4660-4666.
15. Sobczyk-Guzenda, A.; Gazicki-Lipman, M.; Szymanowski, H.; Kowalski, J.; Wojciechowski, P.; Halamus, T.; Tracz, A. *Thin Solid Films* **2009**, *517*, 5409-5414.
16. Renugadevi, R.; Venkatachalam, T.; Narayanasamy, R.; Kirupha S. D. *Optik* **2016**, *127*, 10127-10134.
17. Kajitvichyanukul, P.; Amornchat, P. *Sci. Technol. Adv. Mat.* **2005**, *6*, 344-347.
18. Arconada, N.; Castro, Y.; Duran, A.; Hequet, V. *Appl. Catal. B-Environ.* **2011**, *107*, 52-58.
19. Konishi, J.; Fujita, K.; Nakanishi, K.; Hirao, K. *Chem. Mater.* **2006**, *18*, 6069-6074.

20. Agrios, A. G.; Pichat, P. *J. Photoch. Photobio. A* **2006**, *180*, 130-135.
21. Hathway, T.; Jenks, W. S. *J. Photoch. Photobio. A* **2008**, *200*, 216-224.
22. Zamora, M.; Lopez, T.; Asomoza, M.; Melendrez, R.; Gomez, R. *Catal. Today* **2006**, *116*, 234-238.
23. Hsiang, H. I.; Lin, S. C. *Mat. Sci. Eng. a-Struct.* **2004**, *380*, 67-72.
24. You, X. F.; Chen, F.; Zhang, J. L. *J. Sol-Gel Sci. Techn.* **2005**, *34*, 181-187.
25. Wetchakun, N.; Incessungvorn, B.; Wetchakun, K.; Phanichphant, *S. Mater. Lett.* **2012**, *82*, 195-198.
26. Cooper, I. L.; Egerton, T. A.; Qiu, F. L. *J. Eur. Ceram. Soc.* **2009**, *29*, 637-646.
27. Islam, S. Z.; Rankin, S. E. *Mater. Chem. Phys.* **2016**, *182*, 382-293.
28. Liu, Y. D.; Goebl, J.; Yin, Y. D. *Chem. Soc. Rev.* **2013**, *42*, 2610-2653.
29. Shin, Y.; Exarhos, G. *J. Mater. Lett.* **2007**, *61*, 2594-2597.
30. Bu, S. J.; Jin, Z. G.; Liu, X. X.; Du, H. Y.; Cheng, Z. J. *J. Sol-Gel Sci. Techn.* **2004**, *30*, 239-248.
31. Kajihara, K.; Yao, T. *J. Sol-Gel Sci. Techn.* **2000**, *17*, 173-184.
32. Kajihara, K.; Yao, T. *J. Sol-Gel Sci. Techn.* **2000**, *19*, 219-222.
33. Zarezade, M.; Ghasemi, S.; Gholami, M. R. *Catal. Sci. Technol.* **2011**, *1*, 279-284.
34. Bouazza, N.; Ouzzine, M.; Lillo-Rodenas, M. A.; Eder, D.; Linares-Solano, A. *Appl. Catal. B-Environ.* **2009**, *92*, 377-383.
35. Wang, W. D.; Serp, P.; Kalck, P.; Silva, C. G.; Faria, J. L. *Mater. Res. Bull.* **2008**, *43*, 958-967.
36. Woan, K.; Pyrgiotakis, G.; Sigmund, W. *Adv. Mater.* **2009**, *21*, 2233-2239.
37. Di, J.; Li, S. X.; Zhao, Z. F.; Huang, Y. C.; Jia, Y.; Zheng, H. J. *Chem. Eng. J.* **2015**, *281*, 60-68.
38. Wu, C. H.; Kuo, C. Y.; Chen, S. T. *Environ. Technol.* **2013**, *34*, 2513-2519.
39. Silva, C. G.; Faria, J. L. *Appl. Catal. B-Environ.* **2010**, *101*, 81-89.
40. Silva, C. G.; Sampaio, M. J.; Marques, R. R. N.; Ferreira, L. A.; Tavares, P. B.; Silva, A. M. T.; Faria, J. L. *Appl. Catal. B-Environ.* **2015**, *178*, 82-90.
41. Wang, W. D.; Serp, P.; Kalck, P.; Faria, J. L. *Appl. Catal. B-Environ.* **2005**, *56*, 305-312.
42. Yu, Y.; Yu, J. C.; Yu, J. G.; Kwok, Y. C.; Che, Y. K.; Zhao, J. C.; Ding, L.; Ge, W. K.; Wong, P. K. *Appl. Catal. a-Gen.* **2005**, *289*, 186-196.
43. Eder, D.; Windle, A. H. *J. Mater. Chem.* **2008**, *18*, 2036-2043.
44. Luo, Y. S.; Liu, J. P.; Xia, X. H.; Li, X. Q.; Fang, T.; Li, S. Q.; Ren, Q. F.; Li, J. L.; Jia, Z. *Mater. Lett.* **2007**, *61*, 2467-2472.
45. Kongkanand, A.; Kamat, P. V. *Acs Nano* **2007**, *1*, 13-21.
46. Zhang, X. X.; Deng, C. F.; Xu, R.; Wang, D. Z. *J. Mater. Sci.* **2007**, *42*, 8377-8380.
47. Ajayan, P. M.; Stephan, O.; Redlich, P.; Colliex, C. *Nature* **1995**, *375*, 564-567.
48. Endo, M.; Takeuchi, K.; Tajiri, T.; Park, K. C.; Wang, F.; Kim, Y.A.; Hayashi, T.; Terrones, M.; Dresselhaus, M. S. *J. Phys. Chem. B* **2006**, *110*, 12017-12021.
49. Leino, A. R.; Mohl, M.; Kukkola, J.; Maki-Arvela, P.; Kokkonen, T.; Shchukarev, A.; Kordas, K. *Carbon* **2013**, *57*, 99-107.
50. Wu, C. X.; Xu, J. X.; Li, J. X.; Dong, G. F.; Guan, L. H. *Physica E* **2009**, *41*, 1591-1595.
51. Li, Z.; Lin, W.; Moon, K. S.; Wilkins, S. J.; Yao, Y. G.; Watkins, K.; Morato, L.; Wong, C. P. *Carbon* **2011**, *49*, 4138-4148.
52. Piera, E.; Tejedor-Tejedor, M. I.; Zorn, M. E.; Anderson, M. A. *Appl. Catal. B-Environ.* **2003**, *46*, 671-685.
53. Bouras, P.; Stathatos, E.; Lianos, P. *Appl. Catal. B-Environ.* **2007**, *73*, 51-59.

54. Sonawane, R. S.; Dongare, M. K. *J. Mol. Catal. a-Chem.* **2006**, *243*, 68-76.
55. Zhuang, H. L.; Zheng, G. P.; Soh, A. K. *Comp. Mater. Sci.* **2008**, *43*, 823-828.
56. Serp, P.; Corrias, M.; Kalck, P. *Appl. Catal. a-Gen.* **2003**, *253*, 337-358.
57. Sarkar, S.; Das, P. K.; Bysakh, S. *Mat. Chem. & Phys.* **2011**, *125*, 161-167.
58. Li, X. H.; Niu, J. L.; Zhang, J.; Li, H. L.; Liu, Z. F. *J. Phys. Chem. B* **2003**, *107*, 2453-2458.
59. Abbas, N.; Shao, G. N.; Haider, M. S.; Imran, S. M.; Park, S. S.; Kim, H. T. *J. Ind. Eng. Chem.* **2016**, *39*, 112-120.
60. Altin, I.; Sokmen, M.; Biyiklioglu, Z. *Mat. Sci. Semicon. Proc.* **2016**, *45*, 36-44.
61. Wang, Q.; Jin, R.; Zhang, M.; Gao, S. *J. Alloy. Compd.* **2017**, *690*, 139-144.
62. Wang, J.; Zhao, Y. F.; Wang, T.; Li, H.; Li, C. *Physica B* **2015**, *478*, 6-11.
63. Yang, G. D.; Yan, Z. F.; Xiao, T. C.; Yang, B. L. *J. Alloy Compd.* **2013**, *580*, 15-22.
64. Liu, X. G.; Wang, X. D.; Xing, X.; Li, Q. Y.; Yang, J. J. *Adv. Powder. Technol.* **2015**, *26*, 8-13.
65. Zhu, L. W.; Zhou, L. K.; Li, H. X.; Wang, H. F.; Lang, J. P. *Mater. Lett.* **2013**, *95*, 13-16.
66. Paz, Y.; Heller, A. *J. Mater. Res.* **1997**, *12*, 2759-2766.
67. Nam, H. J.; Amemiya, T.; Murabayashi, M.; Toh, K. *J. Phys. Chem. B* **2004**, *108*, 8254-8259.
68. Zhu, X. L.; Shen, M.; Lobban, L. L.; Mallinson, R. G. *J. Catal.* **2011**, *278*, 123-132.
69. 69 Zhou, L. G.; Shi, S. Q. *Carbon* **2003**, *41*, 613-615.
70. Bessekhouad, Y.; Robert, D.; Weber, J. V.; Chaoui, N. *J. Photoch. Photobio. A* **2004**, *167*, 49-57.
71. Zamora, A.; Lopez, T.; Gomez, R.; Asomoza, A.; Melendrez, R. *Catal. Today* **2005**, *107-08*, 289-293.
72. Yang, G. D.; Jiang, Z.; Shi, H. H.; Xiao, T. C.; Yan, Z. F. *J. Mater. Chem.* **2010**, *20*, 5301-5309.